A compensative model for the angle-dependence of motion estimates in noninvasive vascular elastography

Elizabeth Mercure
Laboratory of Biorheology and Medical Ultrasonics, Centre de Recherche, Centre Hospitalier de l'Université de Montréal (CRCHUM), Montréal, Québec H2L 2W5, Canada

Jean-François Deprez
Laboratory of Biorheology and Medical Ultrasonics, Centre de Recherche, Centre Hospitalier de l'Université de Montréal (CRCHUM), Montréal, Québec H2L 2W5, Canada and CREATIS, UMR CNRS 5515, and INSERM, Lyon, France

Jérémie Fromageau
Laboratory of Biorheology and Medical Ultrasonics, Centre de Recherche, Centre Hospitalier de l'Université de Montréal (CRCHUM), Montréal, Québec H2L 2W5, Canada

Olivier Basset
CREATIS, UMR CNRS 5515, and INSERM, Lyon, France

Gilles Soulez
Institute of Biomedical Engineering, Université de Montréal, Montréal, Québec H3C 3J7, Canada; Department of Radiology, Université de Montréal, Montréal, Québec H2L 4M1, Canada; and Department of Radiology, Radio-Oncology and Nuclear Medicine, Université de Montréal, Montréal, Québec H3C 3J7, Canada

Guy Cloutier
Laboratory of Biorheology and Medical Ultrasonics, Centre de Recherche, Centre Hospitalier de l'Université de Montréal (CRCHUM), Montréal, Québec H2L 2W5, Canada; Institute of Biomedical Engineering, Université de Montréal, Montréal, Québec H3C 3J7, Canada; and Department of Radiology, Radio-Oncology and Nuclear Medicine, Université de Montréal, Montréal, Québec H3C 3J7, Canada

Roch L. Maurice[a]
Institute of Biomedical Engineering, Université de Montréal, Montréal, Québec H3C 3J7, Canada and Department of Radiology, Radio-Oncology and Nuclear Medicine, Centre de Recherche, Centre Hospitalier de l'Université de Montréal (CRCHUM), Montréal, Québec H2L 2W5, Canada

Purpose: Atherosclerosis of peripheral cerebral arteries can lead to stroke either by stenosis formation or plaque rupture. This pathology is initiated by the alteration of arterial wall mechanical properties shown to be assessable by ultrasound elastography. Recently, noninvasive vascular elastography (NIVE) was introduced for noninvasive imaging of the mechanical properties of superficial arteries as markers of vulnerable plaques. However, NIVE motion estimates are angle-dependent, with optimal scanning angle being represented by the alignment of tissue motion with ultrasound beam orientation. The objective of this study was to introduce a model that compensates for such angle-dependence in order to reduce the bias on strain estimates, namely, when investigating longitudinal vessel segments.

Methods: The model is based on the Lagrangian speckle model estimator (LSME) because the LSME assesses the 2D-deformation matrix required to compute the scanning angle.

Results: Experiments on vessel-mimicking phantoms indicated that such a model enables the estimation of scanning angle with less than 3-degrees error. The method was also validated *in vivo* in human carotid arteries where less than 4-degrees error was observed. In both cases, the compensative model estimated the inclination angles with low variability.

Conclusion: Angle-dependence may be an important factor to consider in avoiding potentially distort clinical diagnoses. Results, reported in this article, suggest that the LSME-based compensative model might be considered as a very interesting and promising clinical tool for NIVE applications. © *2011 American Association of Physicists in Medicine*. [DOI: 10.1118/1.3539701]

Key words: atherosclerosis, carotid artery, Lagrangian speckle model estimator (LSME), noninvasive vascular elastography (NIVE), angle-dependence, strain-tensor, axial strain, axial shear

I. INTRODUCTION

I.A. Noninvasive vascular elastography (NIVE)

Noninvasive vascular elastography (NIVE), an ultrasound-based imaging modality, was developed to investigate superficial arterial wall mechanical properties.[1–9] In NIVE, time sequences of 2D radio-frequency (RF) data are recorded transcutaneously, while vascular tissue kinematics is induced by blood flow pulsation. Strain images, also called elastograms, are usually computed with correlation-based,[1,2,4,7,8] optimization-based,[5,6,9] or phase-tracking[3] methods. Other NIVE applications use acoustic radiation force impulses (ARFIs) to generate short-duration bursts of relatively high energy to elicit vascular tissue kinematics. In ARFI, axial displacements are assessed by cross-correlation, and local tissue stiffness is deduced from such relative displacement amplitudes.[10,11]

I.B. Angle-dependence of motion estimates

The accuracy of NIVE motion estimates depends, among several things, on the alignment between tissue-motion and ultrasound beam orientations. When tissue-motion and ultrasound beam orientations coincide, the optimal scanning angle is reached, and unbiased motion estimates can be obtained. However, in some cases, this situation could be difficult to achieve. For example, the view of the imaging vessel can be obscured by an organ or bones or, eventually, the patient can have a surgical scar or a dressing covering a wound, so as a result, it will not be possible to align the probe with the tissue-motion orientation.

On the other hand, strain estimates can be used, under certain conditions, for the assessment of tissue stiffness. Since tissue stiffness is related to certain pathological lesions and then can help guide the clinician toward the appropriate treatment or intervention, it is important to rely on accurate estimation of strain.

To compensate for the angle-dependence of strain measurements, a technique known as *angular compounding* can be applied.[12,13] It consists of combining multiple strain estimates at different scanning angle ranges ($[\theta_n, \theta_{n+1}]$) to construct the proper strain image. However, this method is mainly appropriate to assess cross-section areas of an artery. Indeed, for cross-section vessel data, the alignment between tissue-motion and ultrasound beam orientations can be assumed within each scanning angle range $[\theta_n, \theta_{n+1}]$. On the other hand, with regard to investigating longitudinal segments of arteries, the geometrical context is completely different and this technique will not be appropriate.

I.C. Study objectives

In the present paper, we introduce a compensative model of angle-dependence to reduce the bias in strain estimates for the examination of longitudinal artery segments. In 2D elasticity imaging, assuming affine transformation of a region of interest (ROI) allows us to postulate that its orientation can be assessed; that is on the premise that the four motion components (axial and lateral strain and shear, respectively) of

linear transformation (L) are known.[14] In this respect, the model that is proposed to compensate for the angle-dependence of motion estimates is based on the Lagrangian speckle model estimator (LSME) (Ref. 5) because the LSME allows the assessment of the 2D L matrix.

On the other hand, because of postbifurcation hemodynamic perturbations, the internal carotid is a potential site of atherosclerosis development that requires thorough ultrasound examination for the identification of vulnerable plaques. However, several physical limitations, such as its angular orientation with respect to the skin surface, its deep location, and position posterior to the external carotid, can impede the alignment of the ultrasound beam with the vessel wall motion when scanning the internal carotid.

In addition, aging, combined with hypertension and atherosclerosis, is associated with an increase in the carotid tortuosity and carotid bifurcation angle.[15] Since the target population to be investigated by vascular elastography in order to characterize plaque vulnerability or endothelial dysfunction is old and susceptible to present advanced atherosclerotic diseases, a method to correct probe angulation for strain measurement is needed. As reported in a recent paper that validated a noninvasive elastographic method on healthy subject carotids, the consistency of strain measurements was lower for the internal carotid compared to the common carotid.[9] Such a result gave evidence that the difficulty of imaging the internal carotid leads to biased motion estimates that need to be corrected.

In addition to a vessel-mimicking phantom investigation, the theoretical framework of the "compensative model" was validated *in vivo* in human internal carotid arteries.

II. METHODOLOGY

II.A. Phantom study

As illustrated in Fig. 1, *in vitro* experiments were performed on a homogeneous vessel-mimicking phantom (the term "homogeneous" refers to a plaque-free arterial wall), whose geometry simulated a peripheral artery such as the carotid 8 cm in length with 9.1 mm external and 6.5 mm internal diameters, respectively, that provided a wall thickness of 1.3 mm.[16,17] It consisted of a three freeze-thaw cycle polyvinyl alcohol cryogel (PVA-C) material for which Young's modulus (E) was estimated to be 180 kPa.[18] The solution was made of a concentration of 10% polyvinyl alcohol by weight dissolved in pure water (CAS 7732-18-5) and ethanol homopolymer (CAS 9002-89-5). The PVA-C vessel was pressurized by increments to produce vessel wall deformations. Based on typical physiological parameters (70 pulses/min heart rate and 40 mm Hg pulse pressure gradient) and, assuming a frame rate of 19 images/s for the ultrasound scanner, the intraluminal pressure gradient between two consecutive RF image acquisitions was set to 5 mm Hg (0.67 kPa).

The experimental setup to pressurize the vessel-mimicking phantom and to record RF data is illustrated in Fig. 2. The PVA-C vessel was positioned between two watertight connectors, in a Plexiglas box (label 1) filled with

FIG. 1. Picture of the PVA-made vessel-mimicking phantom.

degassed water at room temperature. Rubber o-rings were used to fasten the vessel onto Plexiglas tubes at both extremities. Intraluminal pressure was induced within the vascular phantom with a syringe pump (label 2) and was measured by a pressure monitor (label 3) connected to an acquisition system (label 4). RF data of the phantom were obtained with a Sonix RP scanner (Ultrasonix, Vancouver, BC, Canada—label 5) that was equipped with a 7 MHz linear array probe (label 6) and had a frame rate of 19 images/s. As illustrated in Fig. 3, longitudinal images of the vessel-mimicking phantom were recorded in the (x,y)-plane, with "y" being the vertical orientation. For this study, the ultra-
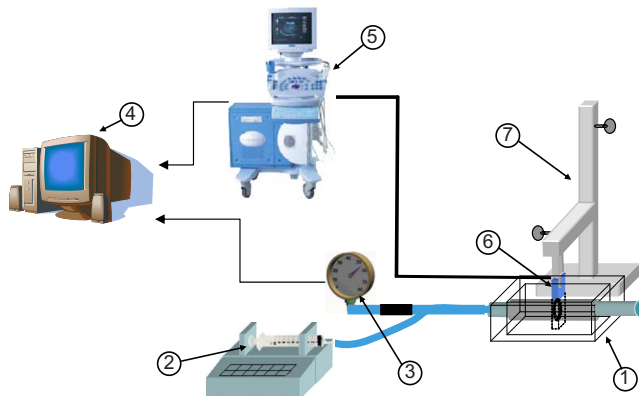

FIG. 2. Schematic illustration of the experimental setup indicating (1) the phantom reservoir, (2) syringe pump, (3) pressure monitor, (4) computer, (5) ultrasound acquisition system, (6) linear array ultrasound probe, and (7) mechanical arm.
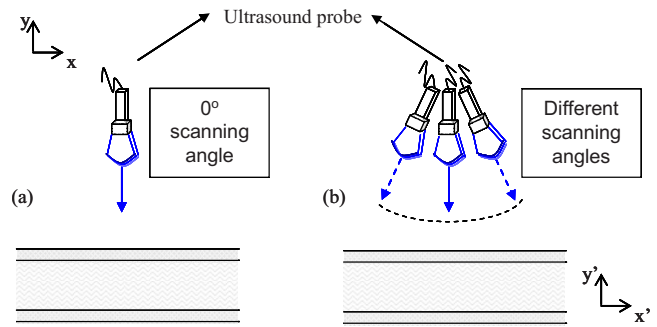
FIG. 3. Schematic representation of a longitudinal vessel segment for 0° scanning angle (a) and for varying scanning angles (b). In (a), the "vessel segment" plane (x',y') coincides with the "ultrasound-image" plane (x,y), i.e. $(x,y)=(x',y')$.

sound probe was fixed to a mechanical arm (label 7 in Fig. 2) that allowed rotational movements simulating different scanning angles. In other words, scanning angle could be defined as rotation of the probe (equivalently the ultrasound beam) with respect to the y axis, with 0°-scanning angle being the case where the ultrasound beam ran parallel to "y."

II.B. *In vivo* study

We are currently conducting a clinical validation of our NIVE method at the CRCHUM. All study subjects signed a written informed consent form approved by the Research Ethics Committee of the CRCHUM.

RF data on longitudinal segments of the internal carotid artery were recorded for several consecutive cardiac cycles with the Sonix RP scanner. The present study comprised of five patients whose (1) internal carotid artery did not exhibit any plaque and (2) ultrasound images displayed an inclination of this vessel of 10° or more. The carotid scans were segmented manually by an expert before elastogram computation. To validate our compensative model, scanning angle was calculated manually on the segmented images by measuring the slope of the arterial wall.

II.C. Tissue-motion model

Vascular tissue is mechanically heterogeneous, and its kinematics can be very complex. Motion within the vessel wall preferably needs to be assessed for small ROI, which are measurement-windows, inside which tissue motion is assumed to be affine.[5] Tissue motion in such ROI was formulated as[5]

$$
\begin{bmatrix} u(t) \\ v(t) \end{bmatrix} = \begin{bmatrix} T_1(t) \\ T_2(t) \end{bmatrix} + \Delta(t) \begin{bmatrix} x \\ y \end{bmatrix},
$$

with

$$\Delta(t) = \begin{bmatrix} \Delta_{xx}(t) & \Delta_{xy}(t) \\[2mm] \Delta_{yx}(t) & \Delta_{yy}(t) \end{bmatrix} = \begin{bmatrix} \dfrac{\partial u(t)}{\partial x} & \dfrac{\partial u(t)}{\partial y} \\[4mm] \dfrac{\partial v(t)}{\partial x} & \dfrac{\partial v(t)}{\partial y} \end{bmatrix}. \tag{1}$$

In Eq. (1), $u(t)$ and $v(t)$ express lateral and axial displacement fields, respectively; $T_1(t)$ and $T_2(t)$ are lateral and axial translation components, respectively; $\Delta(t)$ is the 2D-deformation matrix, with Δ_{xx} and Δ_{yy} being the lateral and axial strain parameters, respectively; and Δ_{xy} and Δ_{yx} being the lateral and axial shear parameters, respectively. It is worth remembering that the axial orientation (y) conventionally coincides with ultrasound beam propagation, whereas lateral orientation (x) is orthogonal to that of the beam.

II.D. The LSME

The LSME (Ref. 5) was used to compute the 2D-deformation matrix Δ given in Eq. (1) between pre- and postmotion RF images. After rigid registration with 2D cross-correlation to compensate for translation movements, i.e. $(T_1(t), T_2(t))$, the LSME was formulated as the following nonlinear minimization problem:

$$\underset{\Delta(t)}{\mathrm{MIN}} \| I(x(t), y(t)) - I_{\mathrm{Lag}}(x(t + \delta t), y(t + \delta t)) \|^2, \tag{2}$$

where $I(x(t), y(t))$ is a premotion small ROI (measurement-window) and $I_{\mathrm{Lag}}(x(t + \delta t), y(t + \delta t))$ is the equivalent postmotion small ROI that was compensated for translations (T_1, T_2). Linear least-squares were used to solve Eq. (2).[20]

In this study, each measurement-window was set to 1540 μm $\times$ 3125 μm, i.e., 80 axial samples $\times$ 20 RF lines, with 94% axial and 90% lateral overlap, respectively. No postprocessing was necessary for *in vitro* elastograms, while a 5 $\times$ 5 pixel median filter was applied to *in vivo* elastograms.

II.E. Scanning angle estimation with the LSME

To compensate for geometric biases that are due to varying scanning angles (θ), θ needs to be estimated. One strategy would be to adjust a cursor on the ultrasound screen parallel to the vessel axis as in pulsed-wave Doppler imaging. A very interesting alternative could be to adopt the LSME that allows 2D-Δ computation and then potential θ estimation.

Because the LSME provides estimates of the deformation matrix within small ROI, the current method aims to estimate θ within each ROI or measurement-window $[I(x(t), y(t))$ in Eq. (2))]. This can be done with the following formulation:[14,19]

$$\theta = \tan^{-1} \left(\frac{\Delta_{yx} - \Delta_{xy}}{(\Delta_{xx} + 1) + (\Delta_{yy} + 1)} \right). \tag{3}$$

In Eq. (3), all four components of the deformation matrix are used. As it has been observed in Ref. 20 that both bias and variability of the lateral components of the deformation matrix (Δ_{xx} and Δ_{xy}) can be quite large, simplifying assumptions

are made to improve the accuracy of angle estimation. Namely, because biological tissues are known to be incompressible,[21] $\Delta_{xx} \approx -\Delta_{yy}/2$ can be hypothesized.[22] Referring to Eq. (1), one can deduce that Δ_{xy} and Δ_{yx} are also of opposite signs. Assuming that ultrasound beams and tissue motion run mostly parallel within the small measurement-windows allows hypothesizing that "$\Delta_{xy} \approx \Delta_{yx} \approx 0$." According to that, Eq. (3) is reformulated as

$$\theta = \tan^{-1} \left(\frac{2\Delta_{yx}}{2 + \Delta_{yy}/2} \right). \tag{4}$$

II.F. Angle-dependence compensative model

Knowing θ, axial strain estimates can then be compensated for angle-dependence. The procedure is geometrically sketched in Fig. 4, where, for simplification and clarity, only the top wall of the vessel segment is represented. As illustrated in Fig. 4(a), Δ_{yy} can be expressed as

$$\Delta_{yy} = \frac{u_y}{l_i}, \tag{5}$$

where u_y is the axial displacement of the inner layer and l_i is the initial dimension of the arterial wall (or wall thickness at a given time). Referring to Fig. 4(c), θ can be defined as the angle between the Eulerian coordinate system (x, y) and the Lagrangian coordinate system (x', y'). (The Eulerian and Lagrangian coordinate systems respectively represent observer and motion coordinate systems.) Such angulation is expected to induce a bias between 0-degree ($\Delta_{yy}{}^0$) or unbiased axial strain and the estimated strain ($\Delta_{yy}{}^\theta$). As shown in Fig. 4(c), if a given point moves from position "A" to "A'," the calculated displacement $u_y{}^\theta$ will be underestimated with respect to 0° displacement $u_y{}^0$. Inversely, calculated length $l_i{}^\theta$ of the vessel wall will be overestimated with respect to its 0° length $l_i{}^0$. The calculated biased axial strain can be obtained with the following simple trigonometric functions:

$$\Delta_{yy}{}^\theta = \frac{u_y{}^\theta}{l_i{}^\theta} = \frac{\cos\theta \cdot u_y{}^0}{l_i{}^0/\cos\theta} = \frac{u_y{}^0}{l_i{}^0} \cos^2\theta = \Delta_{yy}{}^0 \cdot \cos^2\theta. \tag{6}$$

III. RESULTS

III.A. *In vitro* study

One premotion and three postmotion RF images on longitudinal sections of the vessel-mimicking phantom, subjected to a 5 mm Hg (0.67 kPa) intraluminal pressure gradient, were acquired for $\theta = 0°$, 5°, 10°, 15°, respectively. Results reported here then averaged three elastograms for each inclination angle. Only for illustration purposes, Fig. 5 shows axial strain and shear elastograms that were computed for 0° [(a) and (b)] and 15° [(c) and (d)], respectively. Scanning angles were estimated for each measurement-window according to Eq. (3) (method 1) and Eq. (4) (method 2)., i.e. close to 1680 measurement-windows within the top and bottom walls.

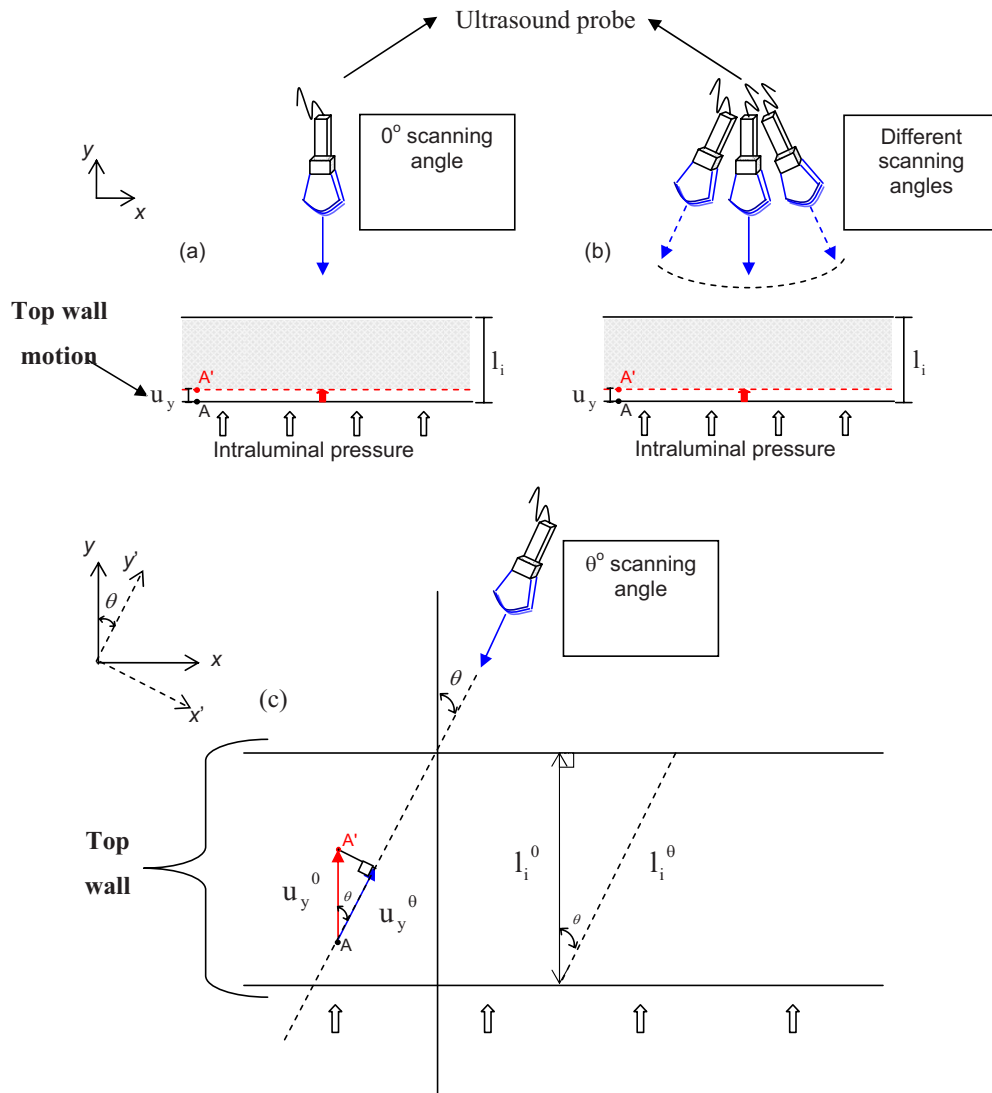The "real" scanning angles were calculated manually on

FIG. 4. Schematic representation of vessel wall kinetics for optimal 0° scanning angle (a) and for varying scanning angles (b). The angle-dependence of axial strain estimates was derived from (c). It is noteworthy that, for simplification, (1) only the top wall is illustrated and (2) translation movements are not represented.

the *in vitro* RF data and were defined as reference angles. Errors between estimated ($\theta_{\text{estimated}}$) and reference ($\theta_{\text{reference}}$) angles were calculated as

$$\text{error} = \theta_{\text{estimated}} - \theta_{\text{reference}}. \tag{7}$$

Means and standard deviations, reported in Fig. 6, were calculated over the whole extent of both proximal and distal walls (1680 measurement-windows) for each inclination angle. Method 1 exhibited very large standard deviations with $\{11.7 \pm 56.1, -18.6 \pm 53.8, 13.8 \pm 43.7,$ and $14.4 \pm 43.9\}°$ instead of $\{-1.3, 4.9, 9.8, 14.5\}°$, manually calculated scanning angles ($\theta_{\text{reference}}$). Such results were predictable due the known inaccuracy and unreliability of lateral motion estimates.[20] On the other hand, method 2 provided pretty accurate estimates of the scanning angles, with low errors and variances for any angle. Indeed, as observed in Table I, it estimated $\{-4.0 \pm 9.3, 5.4 \pm 8.2, 12.4 \pm 9.9, 16.5 \pm 10.9\}°$, whereas $\{-1.3, 4.9, 9.8, 14.5\}°$ were

manually calculated ($\theta_{\text{reference}}$). In summary, method 2 exhibited $\{-2.7, 0.5, 2.6, 2.0\}°$ errors, respectively.

In addition, we also compared, in Table I, axial strain estimates. Strains "corrected with the reference angles" ($\Delta_{\text{reference}}$) consist of a compensation with $\{-1.3, 4.9, 9.8, 14.5\}°$, manually calculated scanning angles, using Eq. (6). For strains corrected with method 2 ($\Delta_{\text{estimated}}$), each strain value (i.e., for each measurement-window) was corrected with the corresponding angle computed with method 2. The bias between these two strain estimates was calculated as

$$\text{bias} = \frac{\Delta_{\text{estimated}} - \Delta_{\text{reference}}}{\Delta_{\text{reference}}} \times 100. \tag{8}$$

The bias was less than 9% for any angle, indicating the reliability of the compensative model. Such a result then suggests that Eq. (4) can reliably be used to correct axial strain estimates for angle-dependence.
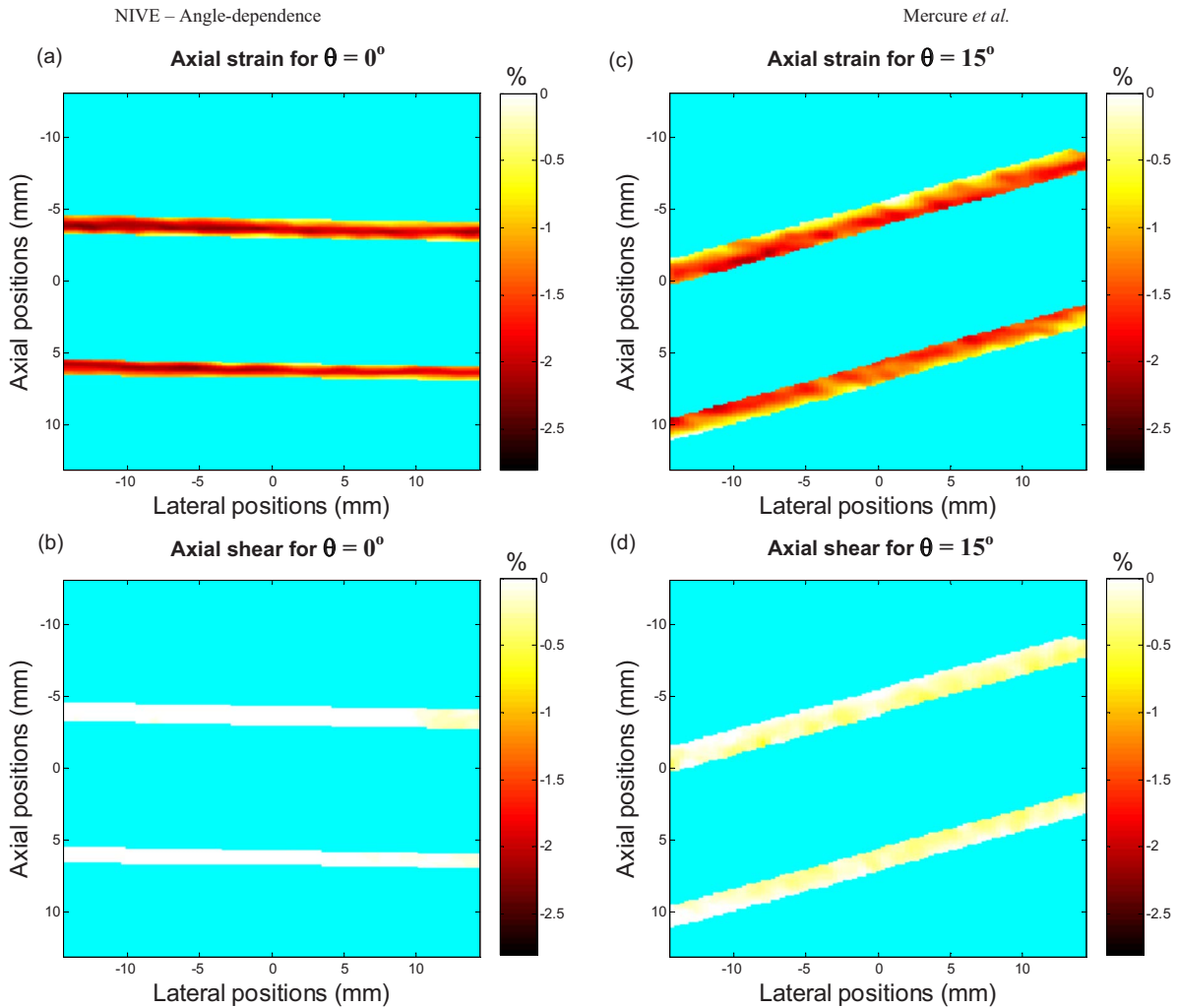
FIG. 5. Axial strain (a) and shear (b) elastograms computed at $\theta=0°$ scanning angle for longitudinal vessel data of the phantom, and axial strain (c) and shear (d) elastograms computed at $\theta=15°$ scanning angle. The color bars express strain and shear values in percent.

III.B. *In vivo* study

A typical example of an *in vivo* ultrasound image of an internal carotid artery is given in Fig. 7. This figure also shows the manual segmentation procedure that allowed the calculation of the scanning angle as the reference method in Table II.

In vivo, the carotid artery is subjected to systolic/diastolic blood flow pulsation. Considering several consecutive cardiac cycles, the data reported in a previous study[9] indicated that peak systolic (PS) and peak diastolic (PD) strain estimates were very stable and reliable. Accordingly, instantaneous PS and PD strain elastograms were used to assess scanning angles. In other words, θ was computed for PS and PD on at least 461 measurement-windows per elastogram, and their absolute values were averaged over three consecutive cardiac cycles.

The data reported in Table II, for five human carotid arteries, indicate that up to $26.8°$ inclination was measured manually. Method 2 estimated $\{12.8 \pm 12.5, \ 15.3 \pm 18.0, \ 14.6 \pm 24.9, \ 18.8 \pm 23.5, \ 28.0 \pm 20.5\}°$ scanning angles instead of $\{13.1, 15.1, 17.6, 22.7, 26.8\}°$, manually calcu-
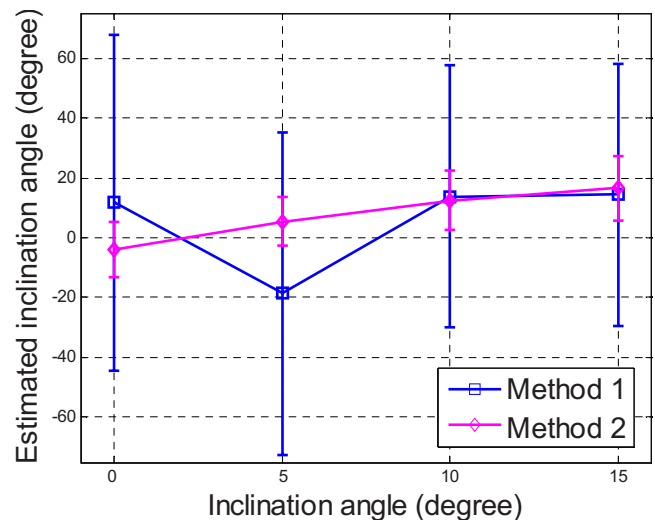

FIG. 6. Means and standard deviations of the scanning angles estimated with Eq. (3) (method 1) and Eq. (4) (method 2).

TABLE I. LSME measurements of scanning angles and of axial strains for the vessel-mimicking phantom. Comparisons are made between method 1, method 2, "nominal," and reference values.

	Scanning angle					Axial strain			
		Method 1		Method 2					
Nominal (°)	Reference (°)	Estimates (°)	Error (°)	Estimates (°)	Error (°)	Estimates (%)	Corrected with reference (%)	Corrected with method 2 (%)	Bias (%)
0	−1.3	11.7	13.0	−4.0	−2.7	1.47	1.47	1.53	4.03
5	4.9	−18.6	−23.5	5.4	0.5	1.46	1.47	1.53	4.03
10	9.8	13.8	4.0	12.4	2.6	1.35	1.39	1.50	7.89
15	14.5	14.4	−0.1	16.5	2.0	1.25	1.33	1.45	8.73

lated. Errors between manual calculation and LSME measurement of the inclination angle were less than 4° for any case. The results obtained with method 1 are not presented due to large standard deviation values ranging from 25 to 51 degrees, as it could be expected. We also compared, in Table II, axial strain estimates that were compensated using the "manually calculated" inclination angles {13.1, 15.1, 17.6, 22.7, 26.8}° and strains that were compensated using method 2. The bias on the strain estimates was 20% or less for any carotid strain measurement. Similar to the *in vitro* study, such a result suggests that Eq. (4) can reliably be used to correct axial strain estimates for angle-dependence.

IV. DISCUSSION

While not restrictive, in this paper, we have introduced a compensative model for angle-dependence with an application in NIVE to investigate longitudinal artery segments. The model is based on the LSME (Ref. 5) because the LSME

FIG. 7. Typical B-mode image of the left internal carotid artery of a patient. Manual segmentation is illustrated.

allows the assessment of the 2D-deformation matrix (Δ) required to compute vessel segment inclination. The theoretical framework was validated on a vessel-mimicking phantom and *in vivo* in human carotid arteries.

Two formulations were proposed to study vessel wall inclination. Method 1, which uses the four components of Δ, was found to be unreliable; that was because of inaccuracy of lateral motion estimates, as expected. Method 2 was determined to be reliable *in vitro* as well as *in vivo*. Comparisons of method 2 with "manual" calculations of inclination angle indicated less than 4-degrees error for any case. In addition, scanning angles were estimated with low variances using this method. Very importantly, comparisons between axial strain estimates that were compensated with "manually calculated" inclination angles (as the reference) and with method 2 showed 20% or less bias for every case, suggesting that the proposed compensative model can reliably be used to correct axial strain estimates for angle-dependence.

It is important emphasizing that to correct strain values with method 2 ($\Delta_{estimated}$), the compensation procedure was applied to each respective measurement-window. Nevertheless, similar to the reference method, it is also possible to compensate the strain value with one single method 2 scanning angle estimate for the whole vessel wall. In such a case, the strain estimate bias would have been less than 5% for any of the five patients presented in Table II.

However, in *real life* situations, the carotid can have tortuous geometries and the data can be recorded at the bifurcation between common and internal carotids. With this respect, the angle between the ultrasound beam and tissue-motion orientations (also said "scanning angle") can exhibit local variations. According to that, we have proposed to correct strain values for each respective measurement-window.

On the other hand, simplifying assumptions were made to enable method 2 angle estimation. We assumed that biological soft tissues were incompressible and then deduced Δ_{xx} from Δ_{yy}, i.e., $\Delta_{xx} \approx -\Delta_{yy}/2$. Nevertheless, in real clinical applications, this can be seen as a coarse approximation of the lateral strain estimate with respect to vascular wall anisotropy. We also assumed that within a measurement-window, lateral and axial shears are close to be additively inversed, i.e., $\Delta_{xy} \approx -\Delta_{yx}$. This can be deemed to be a reasonable assumption, considering the uncertainty in the lateral motion estimates.
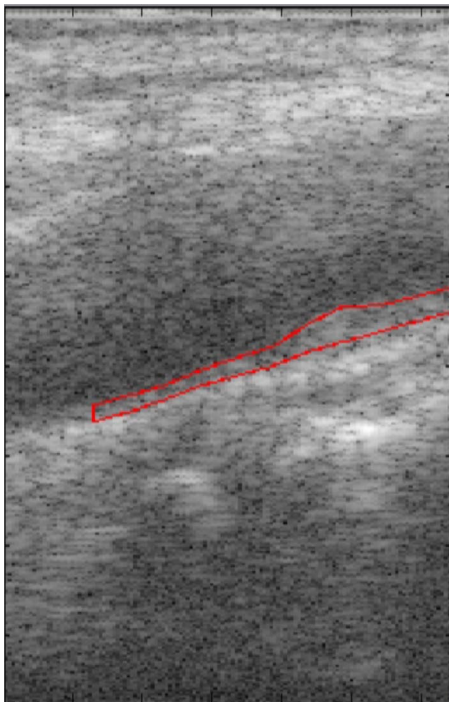
TABLE II. LSME measurements of scanning angles and of axial strains for five internal carotid arteries from five different patients. Comparisons are made between method 2 and reference values.

	Scanning angle			Axis strain			
		Method 2					
Patient No.	Reference (°)	Estimates (°)	Error (°)	Estimates (%)	Corrected with reference (%)	Corrected with method 2 (%)	Bias (%)
1	13.1	12.8	−0.3	0.96	1.01	1.18	16.60
2	15.1	15.3	0.2	0.45	0.48	0.54	11.86
3	17.6	14.6	−3.0	0.47	0.52	0.56	8.26
4	22.7	18.8	−3.9	0.70	0.82	0.99	20.37
5	26.8	28.0	1.2	0.40	0.50	0.55	9.55

However, the compensative model does not take into account estimation biases due to decorrelation noise induced by lateral and transverse motions. Indeed, biases due to decorrelation noise and to vessel angulation can be seen as additive, which may impede the efficiency of the proposed method. Nevertheless, the *in vitro* and *in vivo* data reported in this paper strongly suggest compensating for the angle-dependence of NIVE motion estimates. In addition, Eq. (6) indicates 25% bias for a 30° inclination angle, emphasizing the importance of such a procedure.

In summary, in a previous study, we have reported some pitfalls that could impair NIVE reliability. Namely, the angle-dependence of motion estimates for the internal carotid was pointed out. This paper proposes an interesting solution to that. Based on the LSME, a compensative model is proposed. The results reported for *in vitro* and *in vivo* studies confirm that the LSME-based compensative method might be considered as a very interesting and promising clinical tool for NIVE applications.

V. CONCLUSION

NIVE has already been demonstrated to be a promising method for characterizing human carotid arteries.[5,9] In the current study, theory, supported by *in vitro* and *in vivo* data, suggests that angle-dependence may be an important factor to consider in avoiding any significant bias in the estimation of motion parameters. With this regard, it is worth underlying that aging, combined with hypertension and atherosclerosis, is associated with an increase in the carotid tortuosity and carotid bifurcation angle. Since the target population to be investigated by vascular elastography is old and susceptible to present advanced atherosclerotic diseases, such a compensative method to correct angulation for strain measurement is needed. Indeed, erroneous strain estimates could lead to erroneous evaluation of the arterial wall stiffness and then to inappropriate treatment or intervention. The LSME enables a compensative model for the angle-dependence of motion estimates and might potentially be considered as a very interesting and promising clinical tool for NIVE applications, namely, to investigate the internal carotid.

a)Author to whom correspondence should be addressed. Electronic mail: maurice.roch.chum@ssss.gouv.qc.ca

[1] J. J. Mai and M. F. Insana, "Strain imaging of internal deformation," Ultrasound Med. Biol. **28**, 1475–1484 (2002).

[2] J. Bang, T. Dahl, A. Bruinsma, J. H. Kaspersen, T. A. Hernes, and H. O. Myhre, "A new method for analysis of motion of carotid plaques from RF ultrasound images," Ultrasound Med. Biol. **29**, 967–976 (2003).

[3] H. Kanai, H. Hasegawa, M. Ichiki, F. Tezuka, and Y. Koiwa, "Elasticity imaging of atheroma with transcutaneous ultrasound: Preliminary study," Circulation **107**, 3018–3021 (2003).

[4] K. Kim, W. F. Weitzel, J. M. Rubin, H. Xie, X. Chen, and M. O'Donnell, "Vascular intramural strain imaging using arterial pressure equalization," Ultrasound Med. Biol. **30**, 761–771 (2004).

[5] R. L. Maurice, J. Ohayon, Y. Frétigny, M. Bertrand, G. Soulez, and G. Cloutier, "Non-invasive vascular elastography: Theoretical framework," IEEE Trans. Med. Imaging **23**, 164–180 (2004).

[6] C. Schmitt, G. Soulez, R. L. Maurice, M. F. Giroux, and G. Cloutier, "Non-invasive vascular elastography: Toward a complementary characterization tool of atherosclerosis in carotid arteries," Ultrasound Med. Biol. **33**, 1841–1858 (2007).

[7] H. Ribbers, R. G. Lopata, S. Holewijn, G. Pasterkamp, J. D. Blankensteijn, and C. L. de Korte, "Non-invasive two-dimensional strain imaging of arteries: Validation in phantoms and preliminary experience in carotid arteries *in vivo*," Ultrasound Med. Biol. **33**, 530–540 (2007).

[8] H. Shi, C. C. Mitchell, M. McCormick, M. A. Kliewer, R. J. Dempsey, and T. Varghese, "Preliminary *in vivo* atherosclerotic carotid plaque characterization using the accumulated axial strain and relative lateral shift strain indices," Phys. Med. Biol. **53**, 6377–6394 (2008).

[9] R. L. Maurice, G. Soulez, M. F. Giroux, and G. Cloutier, "Non-invasive vascular elastography for carotid artery characterization on subjects without previous history of atherosclerosis," Med. Phys. **35**, 3436–3443 (2008).

[10] G. E. Trahey, M. L. Palmeri, R. C. Bentley, and K. R. Nightingale, "Acoustic radiation force impulse imaging of the mechanical properties of arteries: *In vivo* and *ex vivo* results," Ultrasound Med. Biol. **30**, 1163–1171 (2004).

[11] D. Dumont, R. H. Behler, T. C. Nichols, E. P. Merricks, and C. M. Gallippi, "ARFI imaging for non-invasive material characterization of atherosclerosis," Ultrasound Med. Biol. **32**, 1703–1711 (2006).

[12] U. Techavipoo, Q. Chen, T. Varghese, J. A. Zagzebski, and E. L. Madsen, "Noise reduction using spatial-angular compounding for elastography,"

IEEE Trans. Ultrason. Ferroelectr. Freq. Control **51**, 510–520 (2004).

[13]H. H. Hansen, R. G. Lopata, and C. L. de Korte, "Noninvasive carotid strain imaging using angular compounding at large beam steered angles: Validation in vessel phantoms," IEEE Trans. Med. Imaging **28**, 872–880 (2009).

[14]M. Bertrand, J. Meunier, M. Doucet, and G. Ferland, "Ultrasonic biomechanical strain gauge based on speckle tracking," IEEE Ultrasonics Symposium, Montreal, pp. 859–863, 1989 (unpublished).

[15]J. B. Thomas, L. Antiga, S. L. Che, J. S. Milner, D. A. Steinman, J. D. Spence, B. K. Rutt, and D. A. Steinman, "Variation in the carotid bifurcation geometry of young versus older adults: Implications for geometric risk of atherosclerosis," Stroke **36**, 2450–2456 (2005).

[16]J. Krejza, M. Arkuszewski, S. E. Kasner, J. Weigele, A. Ustymowicz, R. W. Hurst, B. L. Cucchiara, and S. R. Messe, "Carotid artery diameter in men and women and the relation to body and neck size," Stroke **37**, 1103–1105 (2006).

[17]R. Kazmierski, C. Watala, M. Lukasik, and W. Kozubski, "Common carotid artery remodeling studied by sonomorphological criteria," J. Neuroimaging **14**, 258–264 (2004).

[18]J. Fromageau, J. L. Gennisson, C. Schmitt, R. L. Maurice, R. Mongrain, and G. Cloutier, "Estimation of polyvinyl alcohol cryogel mechanical properties with four ultrasound elastography methods and comparison with gold standard testings," IEEE Trans. Ultrason. Ferroelectr. Freq. Control **54**, 498–509 (2007).

[19]J. Meunier and M. Bertrand, "Echographic image mean gray level change with tissue dynamics: A system-based model study," IEEE Trans. Biomed. Eng. **42**, 403–410 (1995).

[20]E. Mercure, G. Cloutier, C. Schmitt, and R. L. Maurice, "Performance evaluation of different implementations of the Lagrangian speckle model estimator for non-invasive vascular ultrasound elastography," Med. Phys. **35**, 3116–3126 (2008).

[21]T. A. Krouskop, D. R. Dougherty, and F. S. Vinson, "A pulsed Doppler ultrasonic system for making noninvasive measurements of the mechanical properties of soft tissue," J. Rehabil. Res. Dev. **24**, 1–8 (1987).

[22]R. L. Maurice, M. Daronat, J. Ohayon, É. Stoyanova, S. Foster, and G. Cloutier, "Non-invasive high-frequency vascular ultrasound elastography," Phys. Med. Biol. **50**, 1611–1628 (2005).